Available online at www.sciencedirect.com
ScienceDirect
Trans. Nonferrous Met. Soc. China 30(2020) 2724−2736
Transactions of Nonferrous Metals Society of China
www.tnmsc.cn

Interfacial microstructure and mechanical properties of GH99 superalloy and Nb brazed joint using Cu75Pt25 filler

Wen-qiang LI[1], Sheng-peng HU[1,2], Yu-zhen LEI[1,2], Yu LEI[1,2], Xiao-guo SONG[1,2], Ji-cai FENG[2]

1. Shandong Provincial Key Laboratory of Special Welding Technology, Harbin Institute of Technology at Weihai, Weihai 264209, China;
2. State Key Laboratory of Advanced Welding and Joining, Harbin Institute of Technology, Harbin 150001, China

Received 16 July 2019; accepted 7 August 2020

Abstract: Cu75Pt25 brazing filler was applied to brazing GH99 superalloy to Nb, and the sound joints were obtained by adjusting brazing parameters. The typical interfacial microstructure of the brazed joint was Nb/Nb_7Ni_6+$NbNi_3$/Ni(s,s)+Cr-rich $NbNi_3$+($NbCr_2$+$NbNi_3$)/GH99. The effects of brazing temperature and holding time on the interfacial microstructure of GH99/Cu75Pt25/Nb joints were studied. The results showed that the solution and diffusion of Ni atoms from GH99 substrate into brazing seam played a critical role in the interfacial microstructure evolution. As the brazing temperature rose, the Nb−Ni reaction layer was formed instead of the initial Nb_3Pt layer, and the thickness increased firstly and then remained constant. The highest shear strength of the joint reached 152 MPa when brazed at 1150 °C for 15 min. All of the joints presented a brittle fracture mode during shear test, and the fracture location changed from Nb_3Pt layer to Nb−Ni compounds layer.

Key words: nickel-based superalloy; Nb; Cu75Pt25 filler; brazing; microstructure; mechanical properties

1 Introduction

Owing to the attractive properties such as excellent high-temperature strength, corrosion and oxidation resistance, GH99 superalloy has been applied widely in the advanced aeronautic industrial engine combustion chamber and the heat-resistant combustion equipment [1,2]. In practical engineering applications, components utilizing GH99 superalloy and other materials are inevitable. Niobium (Nb) is regarded as an ideal refractory metal material due to its good stability and relatively high strength at high temperature [3,4]. Therefore, reliable joining of GH99 to Nb is a promising work for high-temperature service, such as fuel nozzle and annular combustion chamber in aerospace industry.

Various methods have been utilized to achieve reliable joining of nickel-based superalloys, such as laser welding [5−7], diffusion bonding [8,9] and friction welding [10−12]. Since GH99 alloy contains more elements, the high degree of alloying increases the difficulty of joining to other metals. In fusion welding method [13−15], the intergranular and interdendritic cracking appeared in the fusion zone and heat affected zone (HAZ) of the welded joint owing to the differences of physical properties among dissimilar materials. Compared to the fusion welding method, brazing method possesses good repeatability, simple operation and small thermal impact on the substrates [16], which received great

Foundation item: Projects (51905125, 51775138, U1737205) supported by the National Natural Science Foundation of China; Project (ZR2019BEE031) supported by the Natural Science Foundation of Shandong Province, China; Projects (2017GGX40103, 2019GHY112069) supported by the Key Research and Development Program of Shandong Province, China

Corresponding author: Sheng-peng HU; Tel: +86-631-5677156; Fax: +86-631-5678454; E-mail: sp_hu@hit.edu.cn

DOI: 10.1016/S1003-6326(20)65415-2

attention in joining nickel-based alloy.

Recently, researches have mainly focused on the exploitation of filler alloys suitable for brazing nickel-based superalloys. Nickel-based filler alloys, containing melting point depressant (MPD) elements such as boron, silicon and heat-resistance elements, are considered as the typical high temperature filler metal to braze super-alloys [17−19]. However, the brittle intermetallic compounds, deriving from the reactions between the low-melting-temperature elements of filler metal and nickel-based superalloys, deteriorated the strength of brazed joints [20,21]. In order to overcome this shortage, Cu75Pt25, a novel brazing alloy, aiming to diminish the brittle compounds in the brazing seam was designed. It is noteworthy that copper has good plasticity to release the residual stress produced by different coefficients of thermal expansion of dissimilar materials. As a classic inert metal, the addition of Pt can be conducive to the high-temperature performance of the brazed joint owing to its anti-oxidant properties, high-temperature creep and heat corrosion resistance [22,23].

In this work, GH99 superalloy was brazed to Nb using Cu75Pt25 filler. The influences of brazing temperature and holding time on the interfacial microstructure and mechanical properties of the joints were analyzed in details. In addition, the typical interfacial microstructure and evolution mechanism of brazed GH99/Nb joints were investigated.

2 Experimental

The substrates used in this study were GH99 superalloy and pure Nb. GH99 superalloy was cut into specimens with sizes of 20 mm × 10 mm × 2 mm by wire cut electric discharge machine. The dimensions of Nb substrate specimens were 5 mm × 4 mm × 3 mm. The chemical composition and microstructure of GH99 superalloy are shown in Table 1 and Fig. 1, respectively. Prior to joining, the surfaces to be joined were ground by SiC sandpaper up to 1000-grit and then polished by diamond pastes. The brazing filler of Cu75Pt25 foil was polished to the thickness of 40 μm after being ground with 800-grit SiC sandpapers. According to our previous work [24], Cu75Pt25 filler metal was Cu-based solid solution in microstructure and started to melt at 1127 °C (T_h, solidus temperature) and turned to be liquid at 1170 °C (T_l, liquidus temperature). Subsequently, all of the above polished samples were ultrasonically cleaned in acetone and dried by air blowing. The Cu75Pt25 filler alloy foil was placed between the brazing couple. The assembly diagram of brazed joint is illustrated in Fig. 2(a). A pressure of 1 kPa provided by graphite was applied to ensuring close contact. The vacuum was kept higher than 3.0×10^{-3} Pa in the brazing process.

The samples were firstly heated to 900 °C at a rate of 10 °C/min and held for 10 min, then elevated to the specified brazing temperature at a rate of

Table 1 Chemical composition of GH99 superalloy (wt.%)

Cr	W	Co	Mo	Ti	Al	Fe	Ni
18.32	8.23	6.56	2.93	1.42	1.05	0.31	Bal.

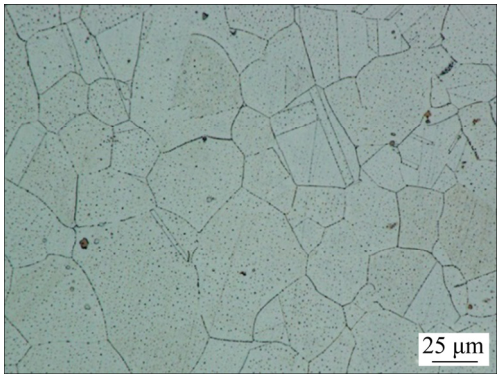

Fig. 1 Microstructure of GH99 superalloy

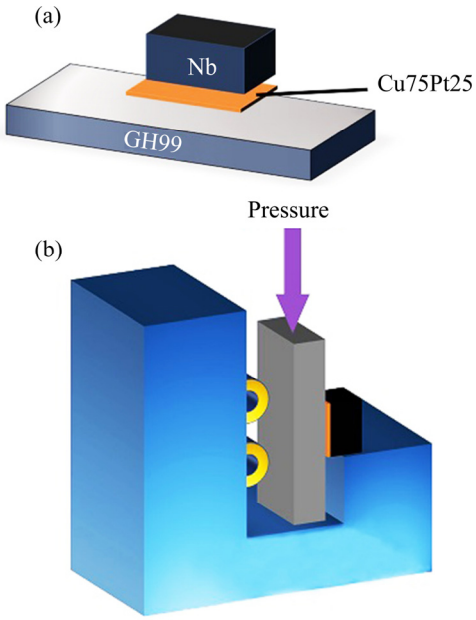

Fig. 2 Schematic diagrams of brazing assembly (a) and shear test (b)

10 °C/min and held for different holding time. At last, the brazed specimens were cooled down to room temperature at a rate of 10 °C/min. The brazing experiment was carried out at 1100, 1120, 1130, 1140, 1150 and 1160 °C, respectively, and the effects of holding time on brazing properties were studied.

The microstructure and composition of brazed joints were analyzed by scanning electron microscope (SEM, MERLIN Compact, Zeiss) equipped with an energy-dispersive spectroscope (EDS, OCTANE PLUS, EDAX). To evaluate the joining properties of brazed joints, room temperature shear tests were performed by the universal testing machine (Instron 5967) with a constant speed of 0.5 mm/min, as shown in Fig. 2(b). At least five samples were tested to average joint strength for each experimental condition. The reactive phases at the interface and fracture morphology of joints after shear test were examined using an X-ray diffractometer (XRD, DX−2700) equipped with Cu K_α radiation.

3 Results and discussion

3.1 Typical interfacial microstructure of GH99/Cu75Pt25/Nb joints

The BSE image in Fig. 3(a) displays the interfacial microstructure of GH99/Cu75Pt25/Nb joint brazed at 1140 °C for 10 min, and the sound joint without any defect such as micro-crack or pore was obtained. The larger thickness of brazing

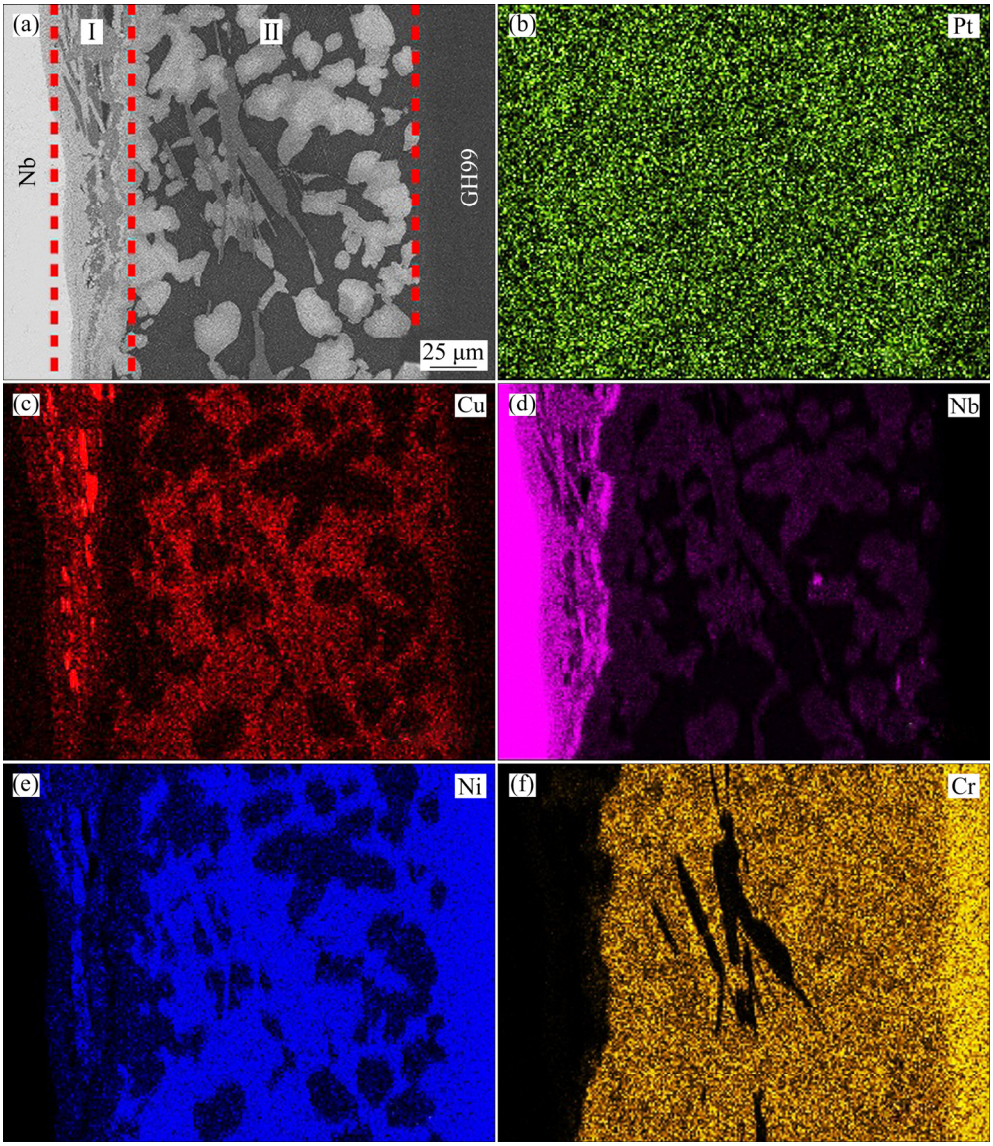

Fig. 3 Interfacial microstructure (a) and element distributions (b−f) of GH99/Cu75Pt25/Nb joints brazed at 1140 °C for 10 min

seam (~200 μm, thicker than that of the filler alloy) indicated the intensive interaction between the molten filler alloy and the substrates during brazing process. According to the difference in the interface, the brazed joint could be divided into two zones (labeled as Zones I and II). Figures 3(b−f) give the distributions of main elements of Pt, Cu, Nb, Ni and Cr, respectively. It is obvious that element Pt is distributed evenly throughout the joint, as shown in Fig. 3(b). Element Cu is also distributed throughout the area of brazing seam, especially enriched in the bits of strip gray-black phase located in Zone I (Fig. 3(c)). A continuous Nb-rich layer (Fig. 3(d)) adjacent to Nb substrate is formed, and mass of lamellar Nb-rich phases are formed in the diffusion zone due to the diffusion of Nb substrate into molten filler alloy, and element Nb also diffuses into the brazing seam, existing in the block composite phases and dark gray lath phase in Zone II. By contrast, element Ni (Fig. 3(e)) is mainly accumulated in the black matrix phase and part of reaction layer in Zone I. The distribution of element Cr (Fig. 3(f)) demonstrates a gradient-decreasing characteristic from GH99 substrate to brazing seam, and it cannot be found in dark gray lath phase for its low solubility. In addition, the mixed phases contain elements Ni, Nb and Cr, and the black matrix mainly consists of element Ni.

According to the contrast difference in Fig. 4, Zone I is made up of continuous reaction layer (marked as A) and multilayer of compounds mixture (marked as B, C, D, E, respectively), and Zone II consists of a small amount of dark gray lath phase (marked as G), composite flocculent structure composed of bright grey, dark grey phases (marked as F and H, respectively) and black matrix phase (marked as J). The corresponding element contents of different spots are listed in Table 2. According to the Nb−Ni binary phase diagram and Refs. [25,26], it can be inferred that the continuous reaction layer A and phase E are Nb_7Ni_6 phase. The molar ratio of Ni to Nb about 3:1 in spots B, C and D is inferred to be $NbNi_3$ phase [27], and the contrast difference of $NbNi_3$ is derived from the contents of solid solution elements Cr and Cu. In Zone II, four typical phases (F, G, H and J) are distinguished visibly. On the basis of the isothermal Ni−Nb−Cr ternary phase diagram and related references [28−32], it can be inferred that the floc-like composite structure (F and H) composed of Nb, Cr and Ni are mainly $NbCr_2$ and $NbNi_3$, respectively. The XRD pattern in Fig. 5 further confirms the above analysis. Likewise, the stoichiometric of Nb/Ni molar ratio of the dark gray lath phase G of about 1:3 is $NbNi_3$ phase, and the black matrix phase J can be identified as

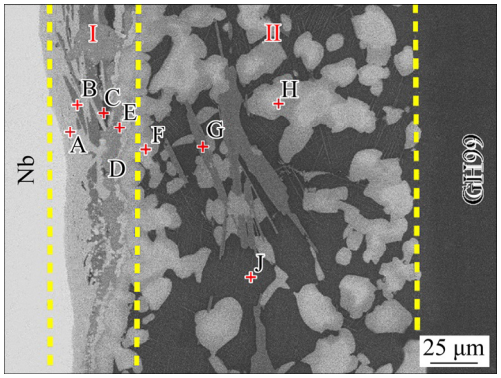

Fig. 4 Interfacial microstructure of GH99/Cu75Pt25/Nb joint brazed at 1140 °C for 10 min

Table 2 Chemical compositions and possible phases of spots in Fig. 4

Spot	Molar fraction/%					Possible phase
	Nb	Ni	Cu	Cr	Pt	
A	52.94	39.09	6.11	1.2	0.66	Nb_7Ni_6
B	22.33	64.34	12.01	0.5	0.82	$NbNi_3$
C	29.35	49.64	10.15	9.54	1.32	$NbNi_3$
D	26.91	60.40	7.83	3.63	1.23	$NbNi_3$
E	47.07	40.24	2.55	6.90	3.24	Nb_7Ni_6
F	28.64	46.41	0.74	23.00	1.21	Cr_2Nb+$NbNi_3$
G	26.57	66.16	1.18	5.73	0.36	$NbNi_3$
H	26.09	48.60	8.38	16.52	0.41	Cr_2Nb+$NbNi_3$
J	0.07	74.68	0.42	23.65	1.18	Ni(s,s)

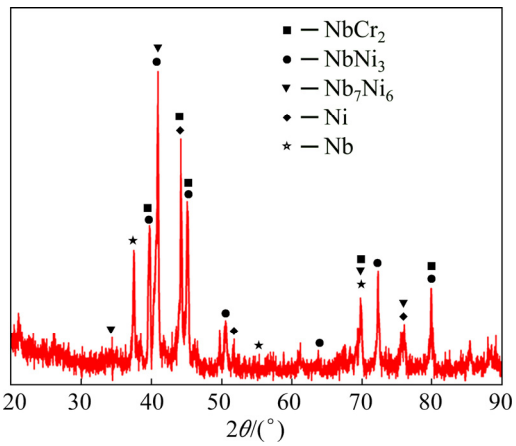

Fig. 5 XRD pattern of GH99/Cu75Pt25/Nb joint brazed at 1140 °C for 10 min

Ni(s,s) [33]. In summary, the typical interfacial microstructure of Nb/Cu75Pt25/GH99 joint is Nb substrate/Nb_7Ni_6 + $NbNi_3$/Ni(s,s) + Cr-rich $NbNi_3$ + ($NbCr_2$+$NbNi_3$)/ GH99 superalloy.

3.2 Effect of brazing parameters on interfacial microstructure of GH99/Cu75Pt25/Nb joints

Figure 6 shows the BSE images of GH99/Cu75Pt25/Nb joints brazed at different temperatures for 10 min, and each joint can be divided into two zones by contrast difference. With the elevation of brazing temperature, the fast atomic diffusion of liquid alloy to Nb substrate led to the increasing width of reaction layer (Zone I). As shown in Figs. 6(a) and (b), the joint interface was even and flat, and the thickness of brazing seam was equal to that of original filler when brazed at 1100 and 1120 °C. When the brazing temperature was above 1127 °C, the thickness of brazing seam increased remarkably (Figs. 6(c−f)), and the elements of Cu and Pt in the filler metal were distributed throughout the joints.

The corresponding high-magnification BSE images of the joints brazed at different temperatures are shown in Fig. 7, and the main phases were characterized by EDS (Table 3). When brazed at

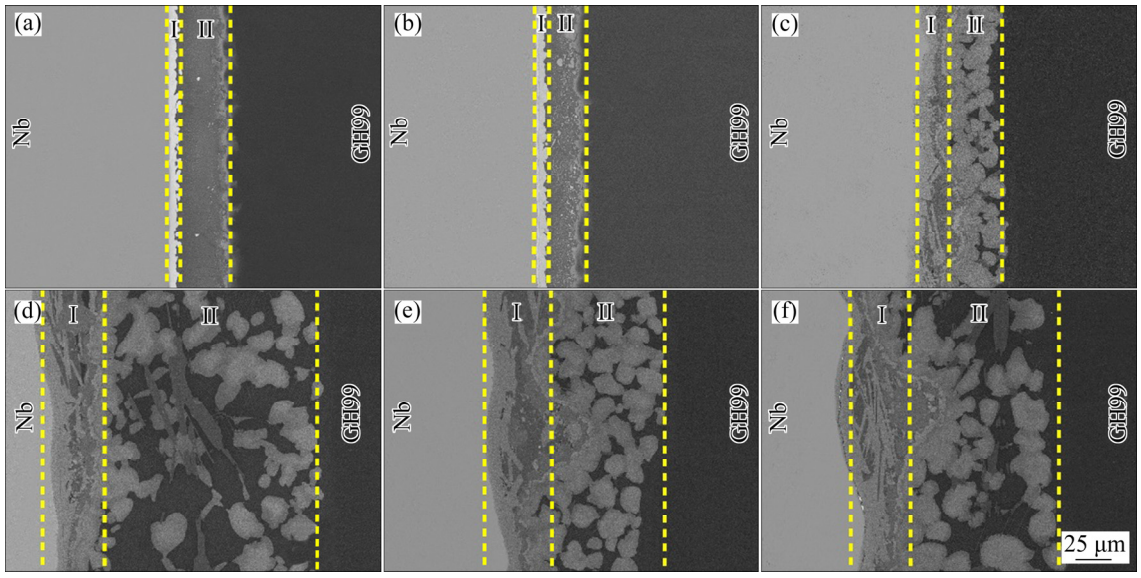

Fig. 6 BSE images of GH99/Cu75Pt25/Nb joints brazed at different temperatures for 10 min: (a) 1100 °C; (b) 1120 °C; (c) 1130 °C; (d) 1140 °C; (e) 1150 °C; (f) 1160 °C

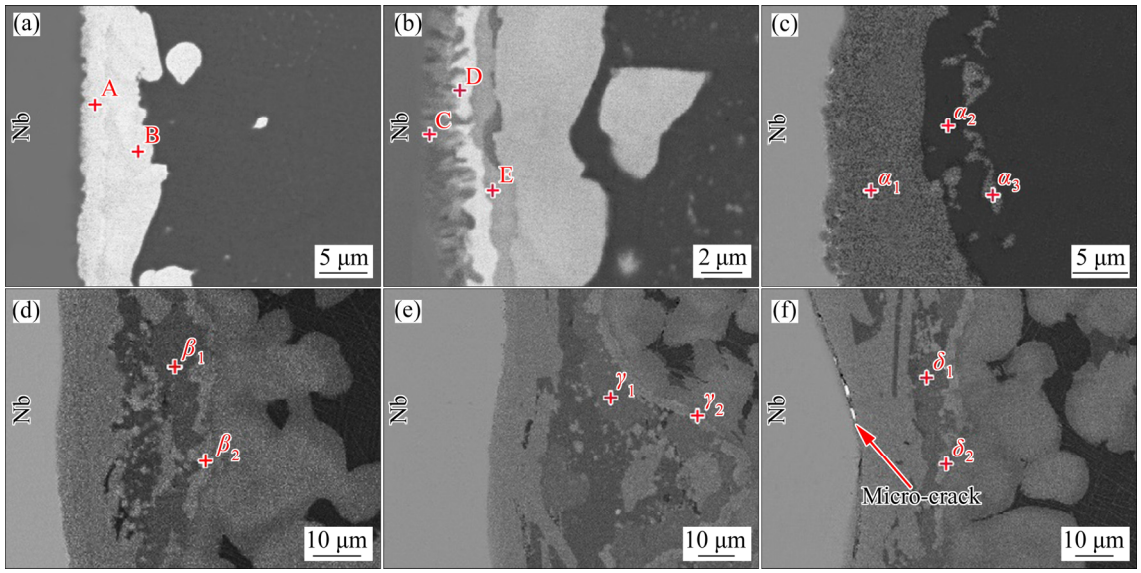

Fig. 7 High-magnification BSE images of GH99/Cu75Pt25/Nb joints brazed at different temperatures for 10 min: (a) 1100 °C; (b) 1120 °C; (c) 1130 °C; (d) 1140 °C; (e) 1150 °C; (f) 1160 °C

Table 3 Chemical composition and possible phases of spots in Fig. 7

Spot or phase	Molar fraction/%					Possible phase
	Nb	Ni	Cu	Cr	Pt	
A	50.86	8.56	8.26	−	32.32	Nb_3Pt
B	25.57	27.37	13.67	−	33.39	Pt(s,s)
C	61.64	25.87	3.62	2.24	6.63	Nb+Nb_7Ni_6
D	62.51	8.82	3.06	4.05	21.56	Nb_3Pt
E	26.60	44.01	10.17	2.57	16.65	$NbNi_3$
α_1	47.66	41.36	5.04	3.37	2.57	Nb_7Ni_6
α_2	35.41	49.70	4.27	9.27	1.35	$NbNi_3$
α_3	52.01	32.04	4.81	7.53	3.61	Nb_7Ni_6
β_1	26.91	60.40	7.83	3.63	1.23	$NbNi_3$
β_2	47.07	40.24	2.55	6.90	3.24	Nb_7Ni_6
γ_1	29.38	49.06	10.08	4.37	7.11	$NbNi_3$
γ_2	47.66	34.33	6.24	4.85	6.92	Nb_7Ni_6
δ_1	30.50	54.76	5.25	8.76	0.73	$NbNi_3$
δ_2	41.81	46.30	5.60	5.88	0.41	Nb_7Ni_6

1100 °C (Fig. 7(a)), Zone I was composed of two distinctive layers with different contrasts, indicating that the reaction layer A was Nb_3Pt phase and layer B phase was Pt(s,s) according to the EDS results and Nb−Ni−Pt ternary phase diagram. When brazed at 1120 °C (Fig. 7(b)), the formed gray and black overlapping phase layer (point C) was similar to the $\alpha_2/\gamma/\alpha_2$ lamellar structure appeared near the TiAl substrate during brazing process [34−36], which could be considered as Nb/Nb_7Ni_6 lamellar structure. Further analysis of points D and E in Fig. 7(b) indicated Nb_3Pt phase and $NbNi_3$ phase according to the EDS results, respectively.

The forming process of Nb/Nb_7Ni_6 lamellar structure was speculated as follows. The dissolution of substrates into molten filler metal and the diffusion of dissolved elements (Ni, Nb, Cr, etc.) from the filler occurred at 1120 °C. Based on the binary phase diagrams of Cu−Nb and Cu−Ni, elements Ni and Cu can form infinite solid solution, while Nb and Cu are almost immiscible. Meanwhile, elements Nb and Ni have larger chemical affinity (−44 kJ/mol) and similar atomic radius (r_{Ni}/r_{Nb}= 0.87). Therefore, a large amount of element Ni and part of Cr in the GH99 side diffused toward Nb substrate side, while only a small amount of element Nb diffused into the brazing seam. The formation of overlapping layer occurred not only because Nb substrate reacted with diffused Ni to form Nb_7Ni_6 at the interface for larger chemical affinity, but also because the residual element Nb remained around Nb_7Ni_6 during the cooling process.

When the brazing temperature was higher than the T_h of Cu75Pt25 filler, the gray-black phase and light gray phase layers (Nb−Ni compounds) in Zone I were formed. In order to investigate the element distributions of the joints at different temperatures, the line scanning analysis was carried out. As shown in Figs. 8, a series of changes occurred with the brazing temperature rising. Firstly, element Cu was gradually distributed from original Cu-rich phase in Zone II to the whole joint, and the distribution of element Pt changed from Nb_3Pt compound at T_1 in Zone I to disperse well in the joints. The disappearance of Nb_3Pt layer was due to the closer electronegativity of Nb and Ni than that of Nb and Pt (the electronegativity values of elements Nb, Ni and Pt are 1.6, 1.8 and 2.2, respectively). Moreover, Pt and Ni are mutually soluble in liquid filler metal, and then Pt can also be dissolved into GH99 substrate. With more components of substrates dissolving into brazing seam, the contents of elements Ni, Nb and Cr in Zone II increased, while the contents of Nb, Ni and Cr in Zone I had no change because the phase

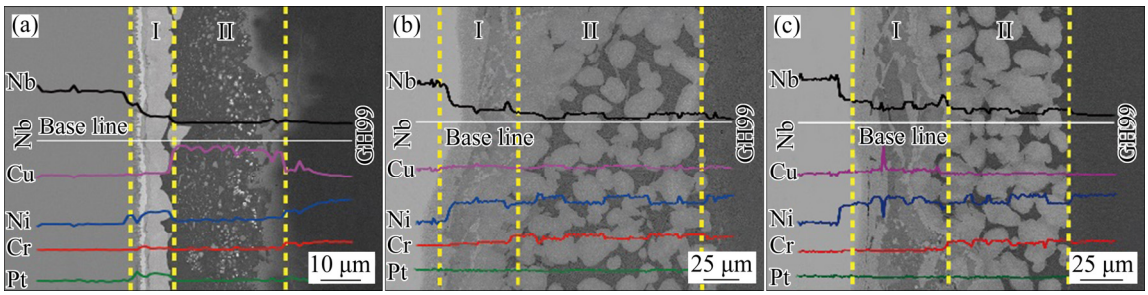

Fig. 8 Interfacial line scanning images of GH99/Cu75Pt25/Nb joints brazed at different temperatures for 10 min: (a) 1120 °C; (b) 1130 °C; (c) 1150 °C

composition of Zone I kept the same after filler alloy melted. Consequently, it was concluded that the distribution and diffusion of elements Cu and Pt were primarily affected by brazing temperature. The phase composition in Zone I changed significantly with the T_h of Cu75Pt25 filler (1127 °C) as the limit.

Figure 9 shows the cross-sectional interfacial microstructures of joints brazed at 1150 °C for different holding time. It is obvious that the width of diffusion zone (Zone II) increased gradually and the thickness of reaction zone (Zone I) increased firstly and then remained constant when the holding time exceeded 10 min. The faster diffusion of numerous elements Nb and Ni could accelerate the interfacial reaction to thicken the Nb−Ni reaction layer. When the holding time reached 20 min, the phases in the joints became coarsening and large amount of roughened strip gray-black $NbNi_3$ phases were formed, and then the thickness of brazing seam was nearly twice thicker than that at 5 min (Fig. 9(d)).

3.3 Interfacial microstructure evolution of GH99/Cu75Pt25/Nb joint

Based on the above discussion about the interfacial microstructure of GH99/Cu75Pt25/Nb joints, the interfacial microstructure evolution of GH99/Cu75Pt25/Nb joint was proposed with the melting temperature (1127 °C) of Cu75Pt25 as the limit, as illustrated in Figs. 10 and 11, respectively.

When the brazing temperature was lower than 1127 °C (Fig. 10), the joint formation could be divided to the following stages. (1) The formation of liquid phase. During the heating process, the local Cu-rich zone in the solid filler metal began to melt, and the micro zone gradually developed to a larger one. (2) The dissolution and diffusion of elements. The formation of liquid phase promoted the elements dissolution, and element Pt dissolved into the molten filler and diffused to Nb substrate to form Nb_3Pt reaction layer. When raising the brazing temperature, element Ni in GH99 substrate dissolved in the molten filler and rapidly diffused to the Nb side for concentration gradient, which promoted the formation of Nb_7Ni_6 phase. Besides, a part of Nb atoms diffused to the solid filler and reacted with Ni atoms to form $NbNi_3$ compounds. (3) The stage of solidification. During the cooling process, the residual molten filler in the brazing seam gradually solidified and precipitated Cu(s,s). Finally, the typical interfacial microstructure of Nb/Nb+Nb_7Ni_6/Nb_3Pt+$NbNi_3$/Cu(s,s)/GH99 was obtained in GH99/Cu75Pt25/Nb brazed joint.

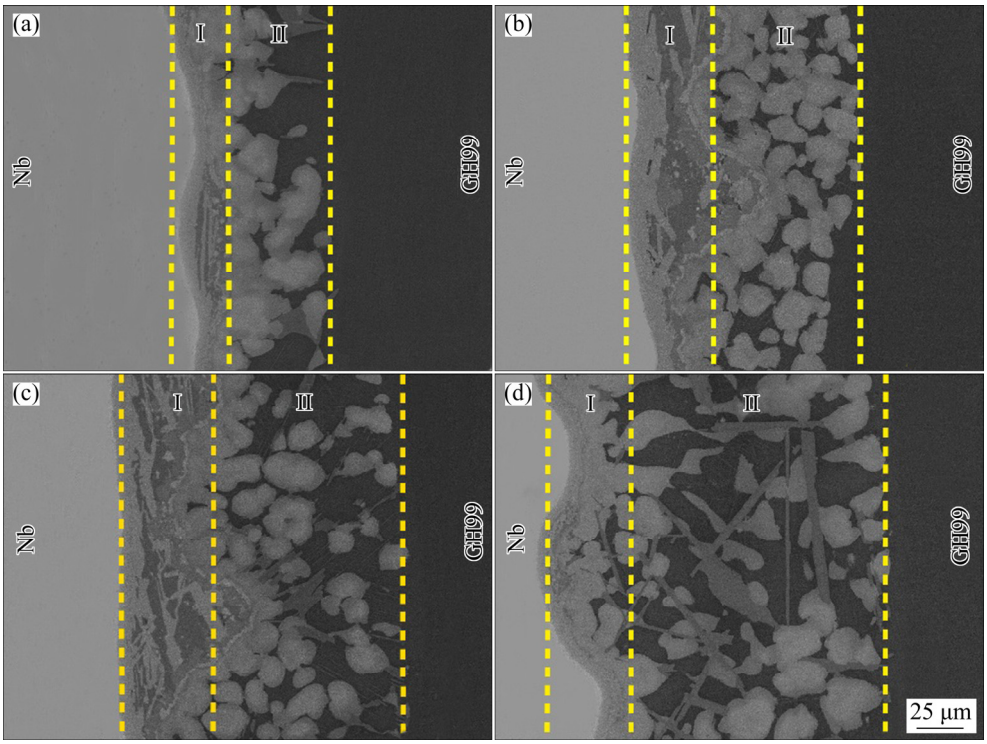

Fig. 9 BSE images of GH99/Cu75Pt25/Nb joints brazed at 1150 °C for different holding time: (a) 5 min; (b) 10 min; (c) 15 min; (d) 20 min

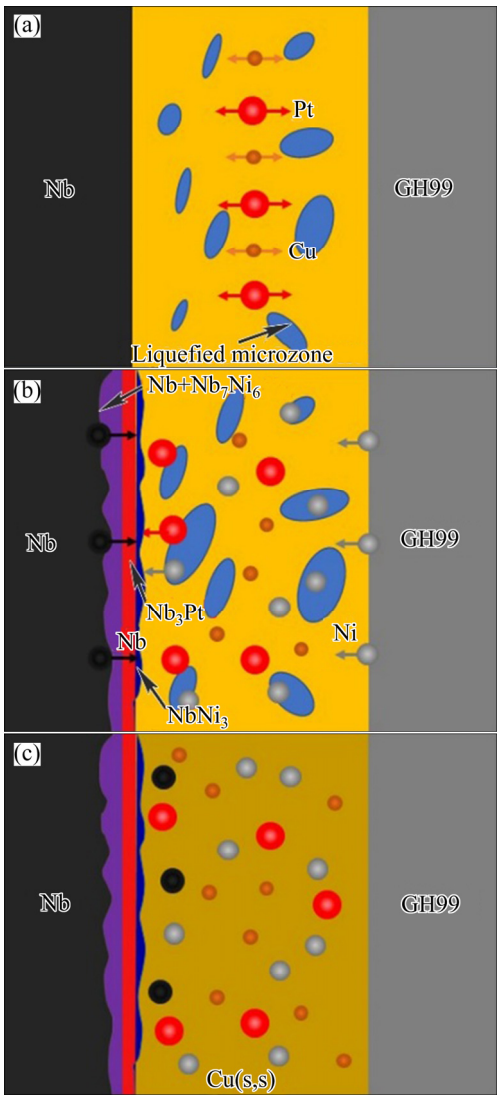

Fig. 10 Schematic formation processes of GH99/Cu75Pt25/Nb brazed joint (<1127 °C): (a) Slow melting of Cu75Pt25 filler; (b) Formation and growth of reaction layers; (c) Formation of interface at cooling stage

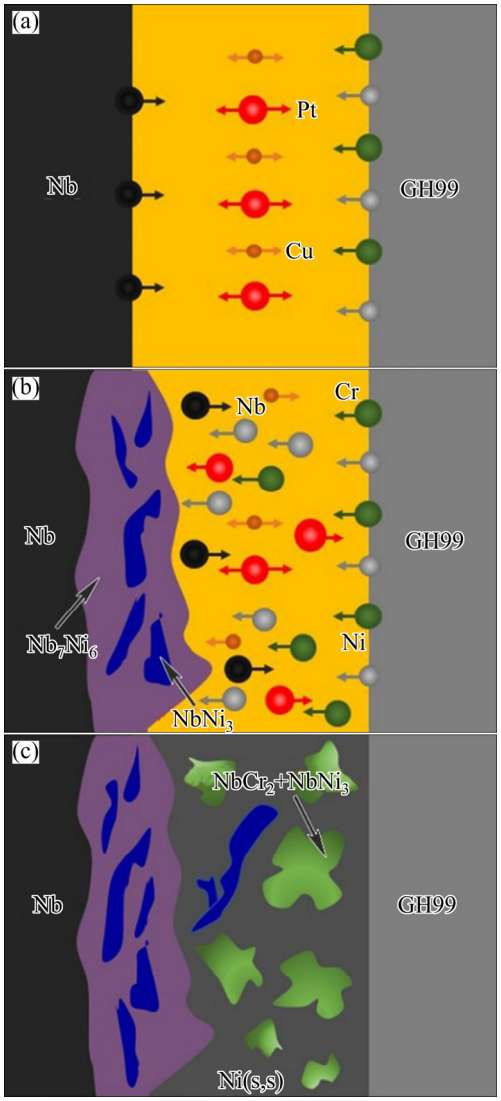

Fig. 11 Schematic formation processes of GH99/Cu75Pt25/Nb brazed joint (>1127 °C): (a) Quick melting of Cu75Pt25 filler; (b) Formation and growth of reaction layers; (c) Formation of interface at cooling stage

When the brazing temperature was higher than 1127 °C (Fig. 11), the joint formation processes were as follows. (1) The formation of liquid phase. The Cu75Pt25 filler metal began to melt and liquid phase was formed when brazing temperature exceeded its melting point. (2) The dissolution and diffusion of elements. Element Ni began to dissolve from GH99 into the liquid. EIJK et al [37] illustrated that element Ni in superalloy diffused into the brazing seam more easily than other alloying elements. Because of the lower partial enthalpy, element Ni has a stronger tendency to react with Nb rather than Pt [38,39], and the Gibbs free energy for the formation of Ni−Nb intermetallics at 880 °C also testified it [40]. Therefore, the formation of Ni−Nb reaction layer was thermodynamically favorable and formed along Nb substrate in the brazing seam (Fig. 11(b)). Meanwhile, the formation of diffusion zone was attributed to the diffusion of elements towards filler metal [41]. Because the diffusion and consumption of element Ni came from GH99, the Ni(s,s) diffusion zone was formed at the GH99 side, which enriched with various alloying elements (Cr, Co, Mo and W). On the other hand, the prolonging holding time led to the strong inter-diffusion of elements Ni and Cr from GH99 and element Nb from Nb substrate to each side [42], which

increased the contents of elements Nb, Ni and Cr in the liquid filler, and the floc-like composite structures ($NbCr_2$ and $NbNi_3$ phases) precipitated during the cooling process. Elements Cu and Pt in the brazing filler were mutually soluble with Ni, leading to their diffusion into GH99 substrate, and then elements Pt and Cu distributed throughout the interface evenly (shown in Figs. 3(b, c)). (3) The stage of solidification. During the cooling process, the liquid phase contained a part of residual elements Ni, Nb and Cr solidified into floc-like composites ($NbCr_2$ and $NbNi_3$ phases), and a small amount of lath Cr-rich $NbNi_3$ phase precipitated in the matrix Ni(s,s). Finally, the typical interfacial microstructure of Nb substrate/Nb_7Ni_6+$NbNi_3$/Ni(s,s)+Cr-rich $NbNi_3$+($NbCr_2$+$NbNi_3$)/GH99 superalloy was formed.

3.4 Effect of brazing parameters on mechanical properties of joints

Figure 12 shows the shear strength of GH99/Cu75Pt25/Nb joints brazed at different brazing parameters. It can be seen clearly that the effects of brazing temperature and holding time on the joining strength are similar. When elevating the temperature and holding time, the shear strengths of the joints increased firstly and then decreased, and the maximum shear strength of ~152 MPa was achieved when brazed at 1150 °C for 15 min.

Figure 13 gives the fractography of GH99/

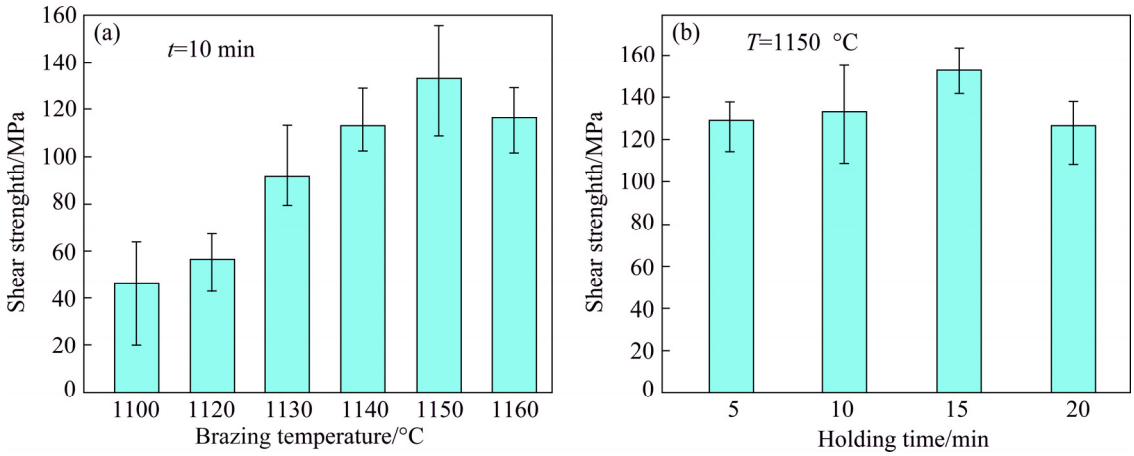

Fig. 12 Effect of brazing parameters on shear strength of GH99/Cu75Pt25/Nb joints: (a) Brazing temperature; (b) Holding time

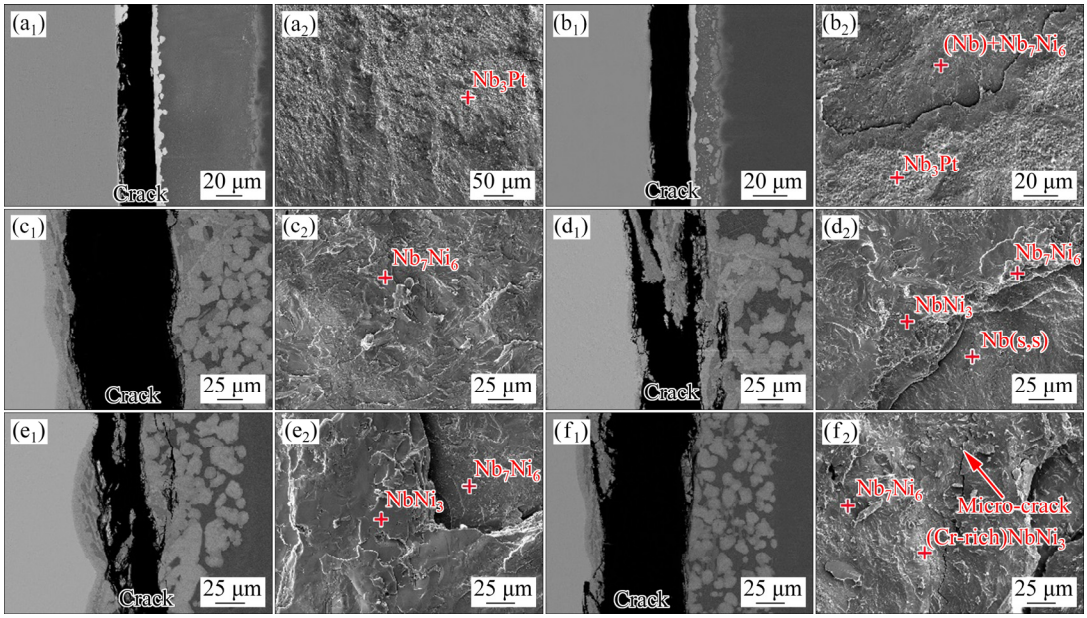

Fig. 13 Brazed joint fracture characterization at 1100 °C (a_1, a_2), 1120 °C (b_1, b_2), 1130 °C (c_1, c_2), 1140 °C (d_1, d_2), 1150 °C (e_1, e_2) and 1160 °C(f_1, f_2) for holding time of 10 min

Cu75Pt25/Nb joints brazed at different temperatures for the same holding time. When the brazing temperature was lower than T_l of Cu75Pt25 filler, the crack mainly occurred in the Nb_3Pt layer and then propagated rapidly to tear part of Nb substrate, as shown in Figs. 13(a_1, b_2). The fracture results indicated the lower bonding strength of Nb substrate/brazing seam interface owing to insufficient element diffusion, and the formation of layered Nb_3Pt brittle phase, which was detected by the XRD pattern (Fig. 14(a)), also deteriorated the joint strength [43,44]. As the brazing temperature increased over T_h, the fracture started from the Nb−Ni intermetallic compound in Zone I and the crack propagated to the Ni-based solid solution along the interface between Zone I and Zone II, as shown in Figs. 13(c_1−f_2). The EDS results of fracture surface showed that the fracture occurred when the Nb_7Ni_6 or $NbNi_3$ phases was formed. The disappeared Nb−Pt compounds were conducive to the improvement of joint strength. However, the increasing solubility of Nb and Ni in the substrates led to the formation of Nb−Ni brittle phases, which was harmful to the joint strength to some extent. In addition, the phases in the brazing seam became coarser and the reaction layer got thicker with the increasing brazing temperature, which also resulted in the degradation of joint strength. Finally, the shear strength of GH99/Cu75Pt25/Nb joints reached the maximum of 133.3 MPa when brazed at 1150 °C.

The fracture morphology in Fig. 15 showed that the fracture mode was the second brittle rupture, as described above at 1150 °C for different holding time. Totally, the effect of holding time on the joining properties was similar to that of brazing temperature. With holding time prolonging, all of the fracture location occurred in Nb−Ni compounds layer close to Nb substrate and the fracture surfaces presented cleavage facet features, as shown in Fig. 15. With further increasing holding time to 20 min, the fracture surface was dominated by larger cleavage surface with small amount of Ni-based solid solution, as shown in Fig. 15(h).

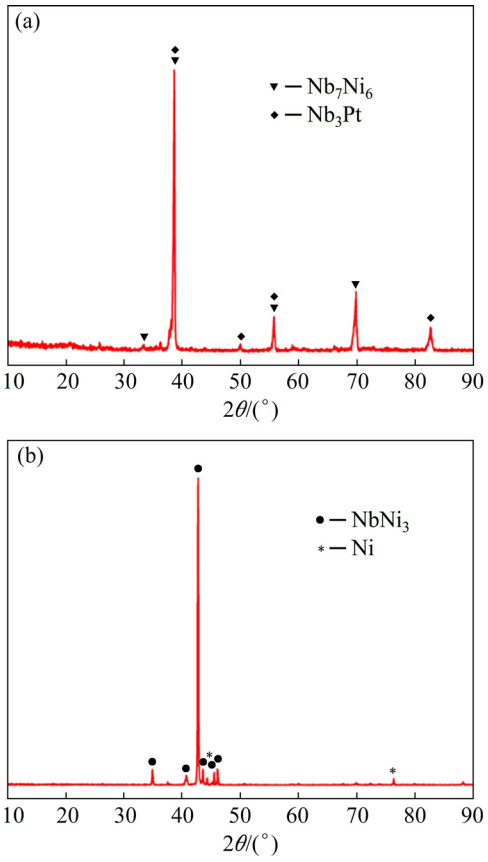

Fig. 14 XRD patterns of fracture surface after shear test of joint brazed at different temperatures for 10 min: (a) 1120 °C; (b) 1150 °C

4 Conclusions

(1) The typical interfacial microstructure of GH99 superalloy and Nb brazed at 1140 °C for 10 min was Nb substrate/Nb_7Ni_6+$NbNi_3$/Ni(s,s)+Cr-rich $NbNi_3$+($NbCr_2$+ $NbNi_3$)/GH99 superalloy.

(2) Brazing temperature and holding time accelerated the inter-diffusion and reaction of elements between molten filler and substrates, which resulted in the increasing thickness of Nb−Ni intermetallic reaction layers and diffusion layer. The thicknesses of diffusion zone and reaction layer on GH99 superalloy side increased gradually with the extension of holding time. With the elevation of brazing temperature, the thickness of Nb−Ni reaction layer that replaced the Nb_3Pt phase formed at low brazing temperature increased firstly and then remained constant.

(3) The shear strength of joints increased firstly and then decreased as the temperature increasing or holding time prolonging. The highest average shear strength reached ~152 MPa when brazed at 1150 °C for 10 min. Cracks tended to initiate and propagate in the brittle Nb_3Pt phase when brazing temperature was lower. The fracture location transformed into the Nb_7Ni_6/$NbNi_3$ layer adjacent to Nb substrate when brazing temperature was higher than 1127 °C.

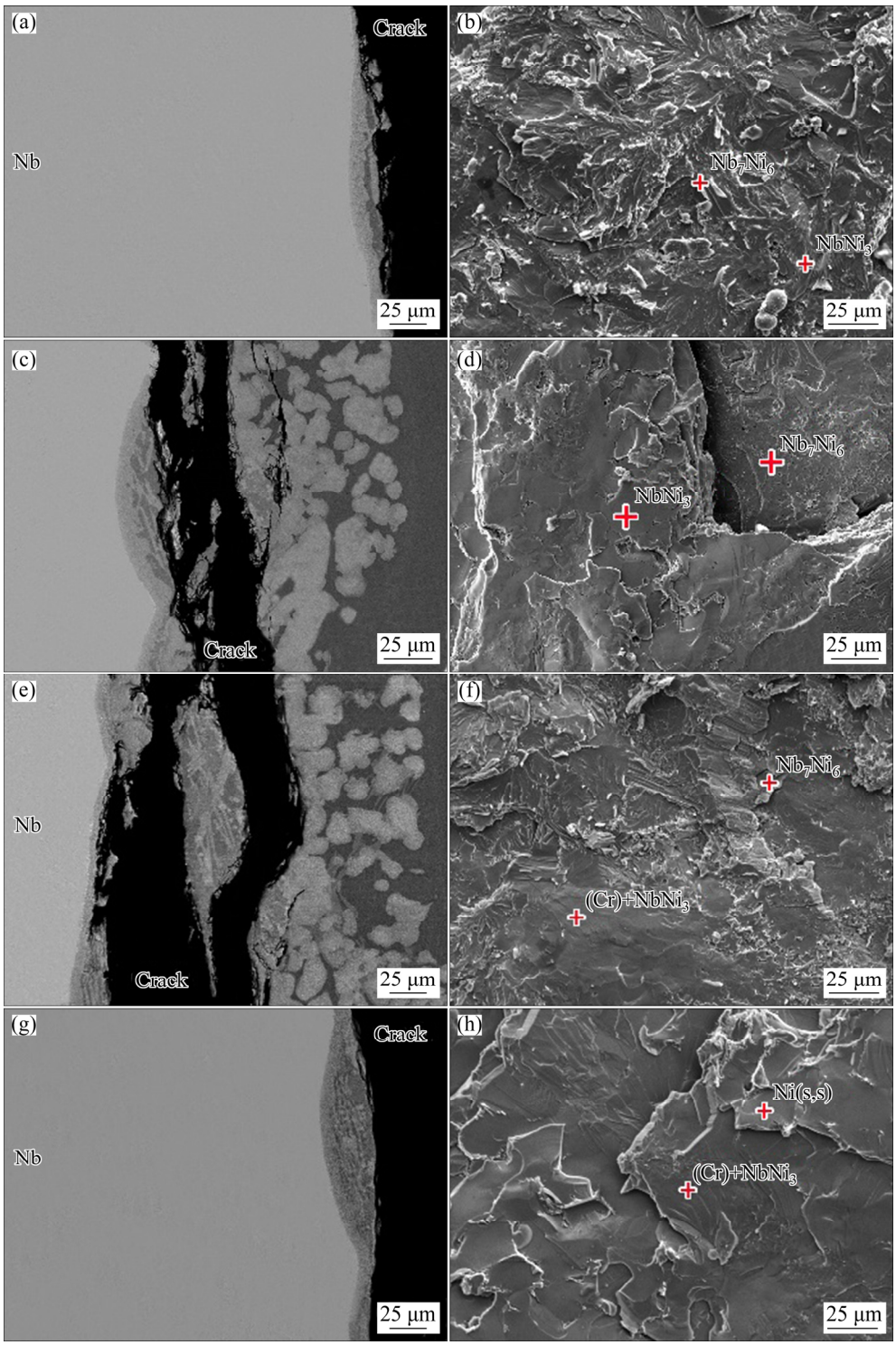

Fig. 15 Brazed joint fracture characterization at 1150 °C for 5 (a, b), 10 (c, d), 15 (e, f) and 20 min (g, h): (a, c, e, g) BSE images of fracture path; (b, d, f, h) Corresponding fracture surface morphologies

References

[1] LIU D, SONG Y Y, SHI B, ZHANG Q, SONG X G, NIU H W, FENG J C. Vacuum brazing of GH99 superalloy using graphene reinforced BNi-2 composite filler [J]. Journal of Materials Science & Technology, 2018, 34(10): 1843−1850.

[2] ZHANG L X, SHI J M, LI H W, TIAN X Y, FENG J C. Interfacial microstructure and mechanical properties of ZrB_2−SiC−C ceramic and GH99 superalloy joints brazed with a Ti-modified FeCoNiCrCu high-entropy alloy [J]. Materials & Design, 2016, 97: 230−238.

[3] ZHANG J, ZHANG Q, LIU C, WANG G, XUAN Y. Effect of brazing temperature on microstructure and mechanical

properties of 2D C_f/SiC and Nb joints brazed with Co−Ti−Nb filler alloy [J]. Materials Science and Engineering A, 2015, 634: 116−122.

[4] YANG Z W, WANG C L, HAN Y, ZHAO Y T, WANG Y, WANG D P. Design of reinforced interfacial structure in brazed joints of C/C composites and Nb by pre-oxidation surface treatment combined with in situ growth of CNTs [J]. Carbon, 2019, 143: 494−506.

[5] PANG M, YU G, WANG H H, ZHENG C Y. Microstructure study of laser welding cast nickel-based superalloy K418 [J]. Journal of Materials Processing Technology, 2008, 207(1−3): 271−275.

[6] ŁYCZKOWSKA K, MICHALSKA J. Studies on the corrosion resistance of laser-welded Inconel 600 and Inconel 625 nickel-based superalloys [J]. Archives of Metallurgy and Materials, 2017, 62(2): 653−656.

[7] AO S S, LUO Z, SHAN P, BU X Z, LIU W D. Microstructure of Inconel 601 nickel-based superalloy laser welded joint [J]. Chinese Journal of Nonferrous Metals, 2015, 25(8): 2099−2107. (in Chinese)

[8] XIONG J, YUAN L, ZHU Y, ZHANG H, LI J. Diffusion bonding of nickel-based superalloy GH4099 with pure nickel interlayer [J]. Journal of Materials Science, 2019, 54(8): 6552−6564.

[9] YEH M S, CHANG C B, CHUANG T H. Diffusion bonding of a superplastic Inconel 718SPF superalloy by electroless nickel plating [J]. Journal of Materials Engineering and Performance, 2000, 9(1): 51−55.

[10] MA T J, CHEN X, LI W Y, YANG X W, ZHANG Y, YANG S Q. Microstructure and mechanical property of linear friction welded nickel-based superalloy joint [J]. Materials & Design, 2016, 89: 85−93.

[11] MA T, YAN M, YANG X, LI W, CHAO Y J. Microstructure evolution in a single crystal nickel-based superalloy joint by linear friction welding [J]. Materials & Design, 2015, 85: 613−617.

[12] HUANG Z W, LI H Y, PREUSS M, KARADGE M, BOWEN P, BRAY S, BAXTER G. Inertia friction welding dissimilar nickel-based superalloys 720Li to IN718 [J]. Metallurgical and Materials Transactions A, 2007, 38(7): 1608−1620.

[13] HAN K, WANG H, PENG F, ZHANG B, SHEN L. Investigation of microstructure and mechanical performance in IN738LC joint by vacuum electron beam welding [J]. Vacuum, 2019, 162: 214−227.

[14] OJO O A, CHATURVEDI M C. Liquation micro fissuring in the weld heat-affected zone of an overaged precipitation-hardened nickel-base superalloy [J]. Metallurgical and Materials Transactions A, 2007, 38(2): 356−369.

[15] OJO O A. Intergranular liquation cracking in heat affected zone of a welded nickel based superalloy in as cast condition [J]. Materials Science and Technology, 2013, 23(10): 1149−1155.

[16] HAN G H, BIAN H, ZHAO H Y, SONG X G, LI Y, LIU D, CAO J, FENG J C. Interfacial microstructure and mechanical properties of TZM alloy and ZrC particle reinforced tungsten composite joint brazed using Ti−61Ni filler [J]. Journal of Alloys and Compounds, 2018, 747: 266−275.

[17] RUIZ-VARGASA J, SIREDEY-SCHWALLER N, GEY N, BOCHER P, HAZOTTE A. Microstructure development during isothermal brazing of Ni/BNi-2 couples [J]. Journal of Materials Processing Technology, 2013, 213(1): 20−29.

[18] ARAFIN M A, MEDRAJ M, TURNER D P, BOCHER P. Transient liquid phase bonding of Inconel 718 and Inconel 625 with BNi-2: Modeling and experimental investigations [J]. Materials Science and Engineering A, 2007, 447(1−2): 125−133.

[19] LIU W S, LIU S H, MA Y Z, CAI Q S, WU L. Microstructure and properties of tungsten/steel joint brazed with Ni-based foil-type filler [J]. Chinese Journal of Nonferrous Metals, 2014, 24(12): 3051−3058. (in Chinese)

[20] JALILVAND V, OMIDVAR H, SHAKERI H R, RAHIMIPOUR M R. Microstructural evolution during transient liquid phase bonding of Inconel 738LC using AMS 4777 filler alloy [J]. Materials Characterization, 2013, 75: 20−28.

[21] COOK G O, SORENSEN C D. Overview of transient liquid phase and partial transient liquid phase bonding [J]. Journal of Materials Science, 2011, 46(16): 5305−5323.

[22] HEIDLOFF A J, van SLUYTMAN J, POLLOCK T M, GLEESON B. Structural stability of platinum-group-metal-modified γ+γ' Ni-base alloys [J]. Metallurgical and Materials Transactions A, 2009, 40(7): 1529−1540.

[23] GAO S, ZHOU Y, LI C F, LIU Z Q, JIN T. Effects of platinum group metals addition on the precipitation of topologically close-packed phase in Ni-base single crystal superalloys [J]. Journal of Alloys and Compounds, 2016, 671: 458−464.

[24] HU S P, HU T Y, LEI Y Z, SONG X G, LIU D, CAO J, TANG D Y. Microstructural evolution and mechanical properties of vacuum brazed Ti_2AlNb alloy and Ti60 alloy with Cu75Pt filler metal [J]. Vacuum, 2018, 152: 340−346.

[25] QIAN J W, LI J L, HOU J B, XIONG J T, ZHANG F S, HAN Z C. Microstructures and mechanical properties of diffusion bonded Ti_2AlNb and GH4169 joints by using Nb+Ni interlayer [J]. Journal of Aeronautical Materials, 2009, 29(1): 57−62.

[26] LONG L J, PENG H L, SHENG Z F, TAO X J, YA L W. Fracture characteristics of vacuum diffusion bonded TA2 titanium to 1Cr18Ni9Ti stainless steel joint with Nb+Ni interlayers [J]. Materials Science Forum, 2009, 620−622: 399−402.

[27] NAFFAKH-MOOSAVY, HOMAM. Microstructural investigation and castability anticipation in modern Ti/Al/Nb-containing nickel-based superalloys [J]. Transactions of Nonferrous Metals Society of China, 2016, 26(6): 1607−1619.

[28] DU Y, LIU S, CHANG Y A, YANG Y. A thermodynamic modeling of the Cr−Nb−Ni system [J]. Calphad, 2005, 29(2): 140−148.

[29] KODENTSOV A A, van LOO F J. Phase relations in the Nb−Ni−Cr system at 1,100 degrees C [J]. Monatsh Chem, 2012, 143(9): 1309−1314.

[30] SAITO S, TAKASHIMA T, MIYAMA K, NARITA T, ZHAO L. Formation of inter-diffusion layer between NiCrAlY coating and Nb substrate during vacuum heat-treatment [J]. Materials Transactions, 2015, 56(3): 367−371.

[31] TAKEYAMA M, LIU C T. Microstructure and mechanical properties of Laves-phase alloys based on Cr2Nb [J]. Materials Science and Engineering A, 1991, 132: 61−66.
[32] VENKATRAMAN M, NEUMANN J P. The Cr−Nb (chromium−niobium) system [J]. Bulletin of Alloy Phase Diagrams, 1986, 7(5): 462−466.
[33] LI H X, PENG H E, LIN T S, PAN F, HUANG Y D. Microstructure and shear strength of reactive brazing joints of TiAl/Ni-based alloy [J]. Transactions of Nonferrous Metals Society of China, 2012, 22(2): 324−329.
[34] SONG X G, CAO J, CHEN H Y, WANG Y F, FENG J C. Brazing TiAl intermetallics using TiNi−V eutectic brazing alloy [J]. Materials Science and Engineering A, 2012, 551: 133−139.
[35] SONG X G, CAO J, LIU Y Z, FENG J C. Brazing high Nb containing TiAl alloy using TiNi−Nb eutectic braze alloy [J]. Intermetallics, 2012, 22: 136−141.
[36] SHIUE R K, WU S K, CHEN Y T, SHIUE C Y. Infrared brazing of Ti50Al50 and Ti−6Al−4V using two Ti-based filler metals [J]. Intermetallics, 2008, 16(9): 1083−1089.
[37] van EIJK D E C, SALLOM Z K, AKSELSEN O M. Microwave brazing of NiTi shape memory alloy with Ag−Ti and Ag−Cu−Ti alloys [J]. Scripta Materialia, 2008, 58(9): 779−781.
[38] WANG J, GUO Q, KLEPPA O J. Standard enthalpies of formation of some Th alloys with Group VIII elements (Co, Ni, Ru, Rh, Pd, Ir and Pt), determined by high-temperature direct synthesis calorimetry [J]. Journal of Alloys and Compounds, 2000, 313: 77−84.
[39] SCHAEFERS K, QIN J, RÖSNER-KUHN M, FROHBERG M G. Mixing enthalpies of liquid Ni−V, Ni−Nb and Ni−Ta alloys measured by levitation alloying calorimetry [J]. Canadian Metallurgical Quarterly, 1996, 35(1): 47−51.
[40] BOLCAVAGE A, KATTNER U R. A reassessment of the calculated Ni−Nb phase diagram [J]. Journal of Phase Equilibria, 1996, 17(2): 92−100.
[41] SONG X G, BEN Y B, HU S P, FENG J C, TANG D. Vacuum brazing high Nb-containing TiAl alloy to Ti60 alloy using Ti−28Ni eutectic brazing alloy [J]. Journal of Alloys and Compounds, 2017, 692: 485−491.
[42] PAN X L, YU H Y, TU G F, SUN W R, HU Z Q. Segregation and diffusion behavior of niobium in a highly alloyed nickel-base superalloy [J]. Transactions of Nonferrous Metals Society of China, 2011, 21(11): 2402−2407.
[43] LI X F, CHEN D, WU Y, WANG M L, WANG H W. Assessment on the structural, elastic and electronic properties of Nb3Ir and Nb3Pt: A first-principles study [J]. AIP Advances, 2017, 7(6):065012.
[44] SEEBOLD R E, BIRKS L S. Elevated temperature diffusion in the systems Nb−Pt, Nb−Se, Nb−Zn, Nb−Co, Ni−Ta, and Fe−Mo [J]. Journal of Nuclear Materials, 1961, 3(3): 260−266.

Cu75Pt25 钎料钎焊 GH99 和 Nb 焊接接头的界面组织及力学性能

李文强[1]，胡胜鹏[1,2]，雷玉珍[1,2]，雷 煜[1,2]，宋晓国[1,2]，冯吉才[2]

1. 哈尔滨工业大学(威海) 山东省特种焊接技术重点实验室，威海 264209；
2. 哈尔滨工业大学 先进焊接与连接国家重点实验室，哈尔滨 150001

摘 要：采用 Cu75Pt25 钎料对 GH99 高温合金与 Nb 合金进行焊接，通过调节焊接参数获得良好的钎焊接头。钎焊接头的典型界面显微组织结构为 Nb/Nb_7Ni_6+$NbNi_3$/Ni(s,s)+富 Cr $NbNi_3$+($NbCr_2$+$NbNi_3$)/GH99。分析钎焊温度和保温时间对 GH99/Cu75Pt25/Nb 接头界面显微组织的影响。结果表明，GH99 合金中 Ni 原子向液态钎料的溶解和扩散对界面组织演化起着至关重要的作用。随着钎焊温度的升高，Nb−Ni 反应层将取代原来生成的 Nb_3Pt 化合物层，且其厚度先增大，然后保持不变。1150 °C 保温 15 min 时，所得钎焊接头的最大抗剪强度为 152 MPa；接头均呈现脆性断裂模式，断裂位置由 Nb_3Pt 层向 Nb−Ni 化合物层转变。

关键词：镍基高温合金；铌；Cu75Pt25 钎料；钎焊；显微组织；力学性能

(Edited by Wei-ping CHEN)